NASA Technical Memorandum 82860

Comparison of Laser Anemometer Measurements and Theory in an Annular Turbine Cascade With Experimental Accuracy Determined by Parameter Estimation

Louis J. Goldman and Richard G. Seasholtz
Lewis Research Center
Cleveland, Ohio

Prepared for the
Symposium on Engineering Applications of Laser Velocimetry
sponsored by the American Society of Mechanical Engineers
Phoenix, Arizona, November 14–19, 1982

NASA

COMPARISON OF LASER ANEMOMETER MEASUREMENTS AND THEORY IN AN ANNULAR TURBINE CASCADE WITH EXPERIMENTAL ACCURACY DETERMINED BY PARAMETER ESTIMATION

Louis J. Goldman and Richard G. Seasholtz

National Aeronautics and Space Administration
Lewis Research Center
Cleveland, Ohio 44135

E-1228

ABSTRACT

Experimental measurements of the velocity components in the blade-to-blade (axial-tangential) plane were obtained within an axial-flow turbine stator passage and have been compared with calculations from three turbomachinery computer programs. The theoretical results were calculated from a quasi three-dimensional inviscid code, a three-dimensional inviscid code, and a three-dimensional viscous code. Parameter estimation techniques and a particle dynamics calculation were used to assess the accuracy of the laser measurements, which allows a rational basis for comparison of the experimental and theoretical results. The general agreement of the experimental data with the results from the two inviscid computer codes indicates the usefulness of these calculation procedures for turbomachinery blading. The comparison with the viscous code, while generally reasonable, was not as good as for the inviscid codes.

INTRODUCTION

The aerodynamic and heat transfer characteristics of advanced high temperature core turbine blading are currently being investigated at the NASA Lewis Research Center. A survey of this comprehensive research program has been reported in (1). One important aspect of this effort is to experimentally determine the flow field within the blading for use in the development, improvement, and verification of three-dimensional turbomachinery computer programs. A benchmark experimental data set for this purpose has been obtained previously (2) for the core turbine stator vane described in (1).

The purpose of this paper is to compare typical experimental velocity measurements (2) with calculations from three turbomachinery computer codes. The theoretical results were obtained from the quasi three-dimensional inviscid TSONIC/MERIDL code (3,4), the three-dimensional inviscid DENTON code (5), and the three-dimensional viscous COOGE code (6). In addition, the accuracy of the laser measurements is assessed by parameter estimation techniques and a seed particle dynamics calculation. Knowledge of the measurement accuracy allows a rational basis for comparison of the experimental and theoretical results.

For the experimental investigation (2), a 0.508-meter diameter, ambient air inlet, full-annular cascade operating near the design critical velocity ratio of 0.78 was employed. Optical access was limited geometrically to the radial direction and, therefore, only velocity components in the blade-to-blade (axial-tangential) plane could be obtained by the fringe-type laser anemometer. Initial measurements of the radial velocity component, with a Fabry-Perot interferometer (7), indicated these components are small for the axial flow turbine vanes tested.

This paper includes a description of the cascade and laser anemometer, the experimental and analytical procedures used, and the results obtained. Typical surveys of velocity magnitude and flow angle obtained at 20, 50, and 80 percent axial chord are presented for radial positions of 10, 50, and 90 percent span. Examples of parameter estimation techniques are presented and used to estimate the uncertainty in the measurement of seed particle velocity magnitude, flow angle, and turbulent stresses. Results of a particle dynamics calculation are also included to estimate how well the seed particles follow the air flow.

NOMENCLATURE

$\underset{\sim}{a}$	vector representing the parameters (p in number)
$\underset{\sim}{a}_0$	vector near solution
$\underset{\sim}{b}$	vector, eq. (4)
$\underset{\approx}{C}$	matrix representing the second derivatives of the function $f(\underset{\sim}{a},t)$, eq. (5)
$\underset{\sim}{d}$	vector representing the data (n in number)
f	function of $\underset{\sim}{a}$ and t
<f>	least-squares value of function
m	number of repeated velocity component measurements (1000)
n	number of mean velocity component measurements
p	number of parameters
R	radial direction, percent of span from hub, fig. 4
S	weighted sum of squares, eq. (1)
s_j^2	variance of the velocity component measurements, m^2/s^2, eq. (11)
t	independent variable of function $f(\underset{\sim}{a},t)$
$\overline{U}$	mean velocity magnitude, m/s, fig. 4
$\overline{U}_j$	mean velocity component, m/s, eq. (10)
U_j	velocity component, m/s, fig. 4
u'	streamwise velocity fluctuation, m/s, fig. 4
V_{cr}	critical velocity (velocity at Mach 1), m/sec
v'	transverse velocity fluctuation, m/s, fig. 4
Z	axial position, percent axial chord from leading edge, fig. 4
$\overline{\alpha}$	mean flow angle measured from axial direction, deg, fig. 4
θ	circumferential position, deg, fig. 4

σ_i^2 variance in measurement of dependent variable $f(\underline{a},t)$

σ_{a_k} standard deviation or uncertainty in parameter a_k, eq. (7)

ϕ_j orientation angle of velocity component (direction of fringe normals), deg, fig. 4

Subscripts:

G gas (air)

P seed particle

APPARATUS AND PROCEDURE

Cascade Facility

A photograph and schematic of the cascade facility are shown in figures 1 and 2, respectively. In operation, atmospheric air is drawn through the inlet section, the blading, the exit section, and then exhausted through the laboratory altitude exhaust system. The cascade was described completely in (2) and briefly below.

The inlet section, consisting of a bellmouth and a short straight section, was designed to accelerate the flow to uniform axial flow conditions at the vane inlet. The bellmouth coordinates are presented in (2).

The test section consisted of a cutout in the outer vane ring which provides access for the laser beams (see figs. 1 and 2). The vanes in this region have been machined to the vane tip radius to permit a window to fit flush with the tip endwall. The glass window (3.2 mm thick) was formed into a cylindrical shape that matched the tip radius by sagging it in a vacuum furnace (2).

The stator vanes, of constant profile from hub to tip, have a height of 38.1 mm and an axial chord of 38.23 mm. The vane aspect ratio and solidity at the mean radius are 1.0 and 0.93, respectively (based on axial chord). Additional geometric information, including the vane coordinates, are given in (2)

The exit section consisted of a dump diffusing section and a flow straightening section. The flow straightener was designed to turn the swirling flow back to the axial direction prior to entering the laboratory altitude exhaust system.

Laser Anemometer

The laser anemometer used for this investigation was a fringe-type, on-axis, backscatter system. A photograph of the laser anemometer is shown in figure 1. A brief description of the laser system is presented below and more completely in (2).

Optics. A schematic of the optical configuration is shown in figure 3. An argon-ion laser (operating at 1.5 W) producing light at a wavelength of 514.5 nm, is first passed through two mode matching lens L1 and L2. These lens were selected to form a probe volume with a $1/e^2$ intensity diameter of 125 μm and with the beam waists at the focal point of lens L3. The beam continues through a beam splitter (described in (8)) which produces two equal intensity beams that lay on a common circular path centered on the optical axis. The beam splitter was mounted on a remotely controlled rotary actuator which allows velocity component measurements to be made along any direction in the axial-tangential plane. The two parallel beams were then focused by lens L3 to cross at the probe volume after reflection by mirror M5. The scattered light from the seed particles passing through the probe volume was collected and focused by lens L4 at the center of a 100 μm diameter pinhole placed in front of the photomultiplier. A circular mask on lens L4 reduces the depth of field of the receiving optics, resulting in an effective probe volume size of about 125 μm diameter (in blade-to-blade plane) by 1 mm long (in the radial direction).

Traversing mechanism. The laser and optics were mounted on a traversing table (figs. 2 and 3) made up of three plates placed one on top of another. The top, middle, and bottom plates allowed motion of the optics in the radial, circumferential, and axial directions, respectively. The axial motion plate was manually positioned while the radial and circumferential motion plates were remotely actuated and controlled.

Seed generator. A commercial aerosol generator was used to atomize a liquid fluorescent dye solution (0.02 molar solution of rhodamine 6G in a 50/50 mixture of benzyl alcohol and ethylene glycol). This technique, described in (9), allows measurements to be made close to the hub, vanes, and window. For the data shown herein, the aerosol from the atomizer was passed through an evaporation-condensation unit before injection into the air flow. It is felt that this produced a narrower size distribution of seed particles and also tended to minimize the agglomeration of liquid droplets.

The size of the seed particles detected in the laser measurement process is extremely important because the difference between the detected seed particle velocity and the true gas velocity is a strong function of the particle size. This difference directly contributes to the error in the measurement of the gas velocity. In (2), the mean detected seed particle diameter was estimated, by three independent aerodynamic methods, to be between 1.1 and 1.4 μm, with a most probable value of 1.2 μm.

Electronics and data processing. The signal from the photomultiplier was processed by a commercial counter-type processor using a 500-MHz clock to measure the duration of eight cycles of the filtered burst signal. Both 5/8 comparison and amplitude sequence validation methods were used for all measurements. The digital time interval data from the processor were sent to a microcomputer, which calculated the mean velocity and the relative standard deviation for a fixed number (1000) of validated bursts. The microcomputer was also used to control the traversing mechanism and to calculate the actual position of the probe volume within the cascade.

Experimental Procedure

To operate the cascade facility, ambient air from the test cell was drawn through the cascade and exhausted into the laboratory altitude exhaust system. The test conditions in the cascade were set by controlling the pressure ratio across the vane row with throttle valves located in the exhaust system. For the reported investigation (2), the hub-static to inlet-total pressure ratio was maintained at a value of 0.65. This corresponds to an exit critical velocity ratio near the design value, at the mean radius, of 0.78.

The location of the laser survey measurements, reported in (2), are shown in figure 4. At midspan, surveys were made at 11 axial planes (every 10 percent axial chord) within the vane passage and at one axial plane about 1/2-axial chord downstream of the vane trailing edge. In addition, surveys were made at radial positions near the hub and tip, at several axial stations, as shown. At a given axial and radial position, laser measurements were taken at 1/3-degree increments across the passage. Measurements at about 600 distinct points in the flow field were obtained. Typical results at 20, 50, and 80 percent axial chord and radial positions of 10, 50, and 90 percent span are presented in

this paper. These survey locations are indicated, in figure 4, by solid symbols.

In general, at a fixed point in the flow, two components of velocity were measured so that the velocity magnitude and flow angle could be calculated. These velocity components were oriented about ±20 degrees from the expected flow direction to minimize incomplete signal biasing errors that can occur in turbulent flows (10) and to allow measurements close to the vane surfaces. To estimate the accuracy of determining the seed particle mean velocity and turbulence parameters, multicomponent velocity measurements were made over a wider range of orientation directions. These multicomponent measurements are described later.

Analytical Procedure

Three turbomachinery computer codes were employed to calculate the velocity field for the core stator vanes tested. The theoretical results were obtained from the quasi three-dimensional inviscid TSONIC/MERIDL code (3,4), the three-dimensional inviscid DENTON code (5), and the three-dimensional viscous DODGE code (6). In addition to the obvious differences in the codes noted above, each treats the leading and trailing edges differently. A brief description of the three codes is given below.

The MERIDL program provides a finite-difference solution on the hub-to-tip midchannel stream surface which is then used in the TSONIC program to obtain a finite-difference solution on a number of blade-to-blade stream surfaces from hub to tip. A quasi three-dimensional solution is obtained by requiring that, for each TSONIC solution, the pressure and suction surface static pressures near the trailing edge be equal. This condition is satisfied by slightly changing (by the user) the downstream whirl distribution for the MERIDL program, redoing the TSONIC solutions, and iterating until the above static pressure equality is satisfied to some tolerance limit. This equality must be satisfied for all the TSONIC solutions simultaneously for a quasi three-dimensional solution to be obtained.

Circular leading and trailing edges are specified in the TSONIC code. The high curvatures in these regions together with the inviscid assumption, produces unrealistically high velocities at the leading and trailing edges. This affects to some extent the flow field calculations in these areas.

The DENTON program is a time marching finite volume solution of the Euler equations. At the downstream boundary the static pressure is specified at the hub and the spanwise pressure variation is calculated by the program assuming zero meridional streamline curvature (simple radial equilibrium).

Cusps are placed at the leading and trailing edges of the vanes to minimize discontinuities in the grid slope. The cusps carry no load and, therefore, periodicity is automatically satisfied by the DENTON program.

The DODGE program solves the Navier-Stokes equation by finite difference techniques. The method uses a split momentum equation which separates the pressure and shear forces into coupled equations. The pressure field is obtained using relaxation methods. The shear or viscous equations are solved by forward spatial marching assuming negligible streamwise diffusion. Alternate relaxation and marching intermediate solutions are used to obtain a converged solution.

Cusps are placed at the leading and trailing edges of the vanes as in the DENTON code. However, because of computer storage limitations, the DODGE program does not strictly enforce the downstream periodicity condition. This would be expected to result in problems with the solution particularly near the trailing edge.

ANALYSIS OF MEASUREMENT ACCURACY

Estimating the accuracy of the laser anemometer measurements consists of basically two independent determinations. First, the accuracy of measuring the seed particle mean velocity and turbulence parameters must be estimated. This is accomplished by applying parameter estimation techniques to a set of experimental data, and is described subsequently. Secondly, a determination of how well the seed particles track or follow the air flow must be made. Both of these potential sources of error effect the ultimate accuracy possible in the laser anemometer measurements. Velocity bias errors are negligible in this investigation because of the low turbulence levels.

Parameter Estimation Technique

Parameter estimation is a general method for determining the parameters or constants appearing in an analytic function so that this function "best" fits a set of experimental data. One simple type of parameter estimation, is the well-known linear least-squares method applied to the straight-line equation. For this example, the parameters to be estimated are the slope and intercept. Generalization of the least-squares technique to nonlinear functions, although not as well known, have been described in many references (11 to 13). In addition to providing an estimation of the parameters, these methods also give an estimate of the parameter accuracy. It is this property that is exploited herein.

In the least-squares method, the weighted sum of the squares of the deviations

$$S = \sum_{i=1}^{n} \left[d_i - f_i(\underset{\sim}{a},t) \right]^2 \Big/ \sigma_i^2 \qquad (1)$$

is minimized to obtain the parameters a_k (p in number) appearing in the function $f(\underset{\sim}{a},t)$ that "best" fits the set of data $\underset{\sim}{d}$. The variance σ_i^2 in the measurement of the dependent variable $f(\underset{\sim}{a},t)$ is assumed to be, at worst, a weak function of the parameters a_k. For linear functions, this minimization procedure results in a set of p linear equations for determining the p parameters. To generalize the least-squares method, the nonlinear function is first linearized by expansion in a truncated Taylor series

$$f(\underset{\sim}{a},t) = f(\underset{\sim}{a}_o,t) + \sum_{k=1}^{p} \left. \frac{\partial f}{\partial a_k} \right|_{\underset{\sim}{a}_o} (a_k - a_{ko}) \qquad (2)$$

The Taylor series expansion is made about $\underset{\sim}{a}_o$, which is assumed to be near the solution. Minimizing the sum of the squares, equation (1), by differentiating with respect to the parameters and equating to zero, again results in a set of p linear equations given by (11),

$$b_j = \sum_{k=1}^{p} C_{jk}(a_k - a_{ko}) \qquad j = 1, \ldots, p \qquad (3)$$

where,

$$b_j \equiv \sum_{i=1}^{n} \left[d_i - f_i(\underset{\sim}{a}_o, t)\right] \left(1/\sigma_i^2\right) \frac{\partial f_i}{\partial a_j}\bigg|_{\underset{\sim}{a}_o} \qquad (4)$$

$$C_{jk} \equiv \sum_{i=1}^{n} \left(1/\sigma_i^2\right) \frac{\partial f_i}{\partial a_j}\bigg|_{\underset{\sim}{a}_o} \frac{\partial f_i}{\partial a_k}\bigg|_{\underset{\sim}{a}_o} \qquad j,k = 1, \ldots, p \qquad (5)$$

and, $\underset{\sim}{d}$ is the set of n data points. Solution of equation (3) for the parameters a_k gives,

$$a_k = a_{ko} + \sum_{j=1}^{p} b_j C^{-1}_{kj} \qquad k = 1, \ldots, p \qquad (6)$$

where, $\underset{\approx}{C}^{-1}$ is the inverse matrix of $\underset{\approx}{C}$. Iterative solution of equation (6) is required if the function $f(\underset{\sim}{a},t)$ is nonlinear. Assuming the errors in the measurements are normally distributed, an estimate of the uncertainty (or standard deviation) of the parameters a_k are given by (11),

$$\sigma_{a_k} = \sqrt{\frac{S}{n-p} C^{-1}_{kk}} \qquad k = 1, \ldots, p \qquad (7)$$

It can be shown (11), that if the variance σ_i^2 is assumed constant, then the determination of the parameters a_k and the uncertainty in the parameters σ_{a_k} are independent of the value of this constant. Over a limited range of the independent variable (which is often the case in experiments) this is not an unreasonable assumption. For the above restriction, this means that the accuracy of measuring the dependent variable need not be known to determine the accuracy of the parameters. Actually, the constant variance of the dependent variable can also be determined by parameter estimation (11).

Application to Laser Anemometer Measurements

To apply the parameter estimation techniques described above to determine the seed particle measurement accuracy, appropriate analytic functions $f(\underset{\sim}{a},t)$ must be identified. This is accomplished by reference to figure 4, which shows a fluctuating velocity at a given instant of time. In the following derivation it is assumed that the flow is stationary and the turbulence level is low so that velocity bias errors are negligible. From geometry, the velocity component U_j at an angle φ_j to the axial direction is,

$$U_j = (\bar{U} + u')\cos(\bar{\alpha} - \varphi_j) - v' \sin(\bar{\alpha} - \varphi_j) \qquad j = 1, \ldots, n \qquad (8)$$

Since the time averages of fluctuating velocity components are, by definition zero, the mean values of the fluctuations are also zero. That is,

$$\frac{1}{m}\sum^{m} u' = \frac{1}{m}\sum^{m} v' = 0 \qquad (9)$$

For m measurement of U_j (1000 herein) the mean value $\bar{U}_j$ is, therefore, given by

$$\bar{U}_j = \frac{1}{m}\sum^{m} U_j = \bar{U}\cos(\bar{\alpha} - \varphi_j) \qquad (10)$$

The required analytic function needed to estimate the accuracy of the mean value of velocity magnitude and flow angle is equation (10). The parameters (of eq. (10)) are, therefore, $\bar{U}$ and $\bar{\alpha}$. The independent variable t is identified with φ_j and the dependent variable $f(\underset{\sim}{a},t)$ with $\bar{U}_j$. In application, n independent (different) values of φ_j are set and n values of the mean velocity component $\bar{U}_j$ determined. Parameter estimation is then applied, as described above, to determine the mean velocity magnitude, flow angle, and an estimate of their accuracy.

The accuracy of the turbulence parameters is obtained by considering the variance s_j^2 in the m measurements of velocity component U_j (fixed φ_j). The variance s_j^2 is defined for this purpose as,

$$s_j^2 \equiv \frac{1}{m}\sum^{m} (U_j - \bar{U}_j)^2 = \frac{1}{m}\sum^{m} \left[u' \cos(\bar{\alpha} - \varphi_j) - v' \sin(\bar{\alpha} - \varphi_j)\right]^2 \qquad j = 1, \ldots, n \qquad (11)$$

or

$$s_j^2 = \overline{u'^2} \cos^2(\bar{\alpha} - \varphi_j) + \overline{v'^2} \sin^2(\bar{\alpha} - \varphi_j) - 2\,\overline{u'v'} \sin(\bar{\alpha} - \varphi_j)\cos(\bar{\alpha} - \varphi_j) \qquad (12)$$

where,

$$\overline{u'^2} = \frac{1}{m}\sum^{m} u'^2; \quad \overline{v'^2} = \frac{1}{m}\sum^{m} v'^2; \quad \overline{u'v'} = \frac{1}{m}\sum^{m} u'v' \qquad (13)$$

Equation (12) represents the required analytic function needed to determine the accuracy of the turbulence parameters $\overline{u'^2}$, $\overline{v'^2}$, $\overline{u'v'}$. These parameters are related to the mean values of the streamwise and transverse normal stresses and the shear stress, respectively. When parameter estimation techniques are applied to equation (12) it is assumed that the mean flow direction $\bar{\alpha}$ is known (i.e., it has been determined from previous application of parameter estimation to the mean velocity component data). It should be noted that equation (12) is linear in the parameters, and iteration is not required for solution of the three parameters.

Seed Particle Dynamics

A particle dynamics calculation was made for this vane geometry, in (2), to determine how well different sized particles track the air flow. The seed particle trajectories were calculated assuming frictional or drag forces on the particles follow Stokes law. The calculations were performed for a mean-radius blade-to-blade surface by a method similar to that described in (14). For these calculations, the seed particles are assumed spherical, of known size, and moving through a known air flow field (results from the TSONIC/MERIDL code were used to define the known flow field). The calculated differences in both the magnitude and direction of the seed particles and the air flow indicate how well the seed particles (of assumed size) will track the air flow.

RESULTS AND DISCUSSION

Seed Particle Measurement Accuracy

The accuracy of measuring the seed particle mean velocity and turbulence parameters were determined by the method described in the Parameter Estimation Technique section. The results of this technique, applied to a set of data obtained at 50 percent axial chord and 50 percent span, are shown in figures 5 and 6.

The mean velocity component measurements $\bar{U}_j/V_{cr}$ as a function of the orientation angle φ_j (see fig. 4) are presented in figure 5(a), and the normalized residuals (difference of the data and the least-squares values) are shown in figure 5(b). The solid line in figure 5(a) (eq. (10)) was determined by parameter estimation and gave a least-squares value for mean velocity magnitude $\bar{U}/V_{cr}$ of 0.600 and for mean flow angle $\bar{\alpha}$ of 33.7 degrees. More importantly, the estimated uncertainties calculated from equation (7), for 95 percent confidence interval (2 sigma value), are 0.5 percent in mean velocity magnitude and 0.4 degree in mean flow angle.

Generally, multi-component measurements of this type are not feasible for the whole flow field due to the large time requirements. For the more conventional two-component type of measurement used primarily in this investigation, the measurement uncertainty can also be estimated from parameter estimation. To do this, parameter estimation is first used to determine the assumed constant uncertainty in the dependent variable (11). Prediction analysis (11) is then applied (using this constant uncertainty) to estimate the uncertainty in the parameters for the two-component type of measurement. Using the above method, the uncertainty in the two-component type of measurement is estimated to be 1.0 percent in mean velocity magnitude and 1.4 degree in mean flow angle.

The normalized residuals for the velocity component least-squares fit, shown in figure 5(b), are random about zero indicating a good representation of the data. A case where this was not so, was shown in (10), and was caused by incomplete signal bias. This type of bias did not occur in the measurements reported herein because of the lower turbulence levels.

The normalized standard deviations of the velocity component measurements $s_j/\bar{U}$ as a function of the orientation angle φ_j are presented in figure 6(a), and the normalized residuals are shown in figure 6(b). The solid line shown in figure 6(a) (eq. (12)) was determined by parameter estimation. The least-squares values obtained for the streamwise normal stress $\sqrt{\overline{u'^2}}/\bar{U}$, the transverse normal stress $\sqrt{\overline{v'^2}}/\bar{U}$, and the shear stress $\overline{u'v'}/\bar{U}^2$ are 0.037, 0.036, and 0.0008, respectively. The estimated uncertainties in these measurements are, for 95 percent confidence interval, 6 percent in streamwise normal stress, 10 percent in transverse normal stress, and 22 percent in shear stress. It should be noted, that a few large particles lagging the flow can seriously affect the determination of the turbulence parameters. It is, therefore, important that these biased values be identified and eliminated during data acquisition. Also, the fluctuations due to noise must be smaller than those due to turbulence, for these measurements to approximate the true turbulence parameters of the flow.

The normalized residuals, shown in figure 6(b), for the normalized standard deviation least-squares fit, again show randomness about zero, indicating a good representation of the data.

Seed Particle Lag

The results of the seed particle dynamics calculation at the mean-radius are shown in figure 7. The calculations assume a particle diameter of 1.2 μm which was determined (2) to be the most probable size of partcles detected in the laser measurement process. The results are shown as contour plots of the difference in velocity magnitude and flow direction between the seed particles and the air flow. Generally, the velocity magnitude differences are less than 2 percent and the flow direction differences are less than 1 degree. The seed particles, typically, have lower velocity magnitudes and lower flow angles.

Laser Anemometer Measurements and Comparison with Theory

Typical laser survey measurements are presented in figures 8 to 10 for constant axial positions of 20, 50, and 80 percent of axial chord, respectively. Results at radial positions of 10, 50, and 90 percent span are shown in these figures by offsetting the critical velocity ratio axis while maintaining the circumferential position axis fixed. The experimental measurements are compared with calculations obtained from the three turbomachinery computer codes described in the Analytical Procedure section. The theoretical results shown were determined from the quasi three-dimensional inviscid TSONIC/MERIDL code, the three-dimensional inviscid DENTON code, and the three-dimensional viscous DODGE code. Also shown in the figures, are the calculated free-stream critical velocity ratio near the vane surfaces, which were obtained from vane surface static pressure measurements reported in (15) and (2).

20 percent axial chord surveys. At 20 percent axial chord, figure 8, the experimental data are seen to be generally very smooth, although some scatter is noted at 90 percent span. A comparison of the data and the theoretical results indicate that the agreement at 20 percent axial chord is generally good. The only major disagreements noted are with the the DODGE code velocity results near the suction surface and with all three theoretical calculation of flow angle at 90 percent span. The vane surface static pressure results are also seen to agree well with both the data and the inviscid calculations.

To obtain a more quantative comparison, the experimental data were first corrected for seed particle lag. The theoretical results were then compared with these corrected values to determine (numerically) if they fell within the total measurement uncertainty. The total uncertainty consisted of the errors in measuring the particle velocity (determined by parameter estimation) and errors in estimating the particle size (±0.2 μm). Velocity bias errors were negligible because of the low turbulence levels in this investigation. For the above comparisons, an average value was determined so that the different theoretical calculations could be more easily compared.

At 20 percent axial chord, the TSONIC/MERIDL, DENTON, and DODGE results were found to fall outside the uncertainty band for velocity magnitude by 1.0, 0.4, and 3.7 percent, respectively. All three theoretical calculations fell within the uncertainty band for flow angle.

50 percent axial chord surveys. At 50 percent axial chord, figure 9, the experimental data are seen to contain more scatter than at the previous axial position. This is felt to be due to the higher flow turbulence levels observed at this location. The theoretical velocity variation across the passage was the largest for this region of the flow and was confirmed by the laser measurements. The theoretical flow angle variation across the passage exhibits a minimum between the suction and pressure sides, and this is also seen in the data. The agreement between the laser measurements and theory at 50 percent axial chord is considered to be good. The largest differences noted are with the flow angle at 90 percent span. The vane surface static pressure results agree well with the experimental data and with the theoretical inviscid results, but are higher than the DODGE code values near the suction surface.

At 50 percent axial chord, the TSONIC/MERIDL, DENTON, and DODGE results were found to fall outside the uncertainty band for velocity magnitude by 0.5, 0.7, and 1.5 percent, respectively. Corresponding results for the flow angle calculations, indicated that they fell outside the uncertainty band by 0.1, 0.1, and 0.8 degree, respectively.

80 percent axial chord surveys. At 80 percent axial chord, figure 10, the experimental data scatter are similar to the previous axial position and is also felt to be caused by the higher turbulence levels at this location. The theoretical variations in velocity and flow angle across the passage were smaller at this axial position, and the data also exhibit this behavior. However, larger differences in the velocity results for the three theoretical codes are noted. The agreement between the data and the DENTON code is considered good while the comparison with the other two codes is only fair. The larger differences seen at this axial position are felt to be caused by the modeling of the trailing edge region in the computer codes. This was discussed previously in the Analytical Procedure section. The vane surface static pressure results agree reasonably well with both the data and with the inviscid code results.

At 80 percent axial chord, the TSONIC/MERIDL, DENTON, and DODGE results were found to fall outside the uncertainty band for velocity magnitude by 2.0, 0.4, and 2.9 percent, respectively. Corresponding results for the flow angle calculations, indicated that they fell outside the uncertainty band by 0.1, 0.2, and 1.7 degree, respectively.

Similarly, the overall passage averaged value for the TSONIC/MERIDL, DENTON, and DODGE results were found to fall outside the uncertainty band for velocity magnitude by 1.1, 0.5, and 2.7 percent, respectively. Corresponding results for flow angle, indicated that the DODGE calculations fell 0.8 degree outside, while the TSONIC/MERIDL and DENTON calculations fell within the uncertainty band. Therefore, the best agreement between the data and theory (on an average basis) is shown for the DENTON code. The larger differences noted for the DODGE code are felt to be caused by lack of the program to strictly enforce the downstream periodicity condition.

CONCLUSIONS

(1) The general agreement of the laser anemometer measurements with the results from two inviscid computer programs indicates the usefullness of these calculation procedures for turbomachinery blading. The best agreement was found for the three-dimensional inviscid DENTON calculations. The comparison with the three-dimensional viscous DODGE code, while generally reasonable, was not as good as for the inviscid codes.

(2) Parameter estimation techniques, at 50 percent axial chord and 50 percent span, indicated seed particle measurement uncertainties of 1.0 percent in velocity magnitude, 1.4 degrees in flow angle, 6 percent in streamwise normal stress, 10 percent in tranverse normal stress, and 22 percent in shear stress.

(3) A particle dynamics calculation indicated that the differences between the seed particles and the air flow would generally be less than 2 percent in velocity magnitude and less than 1 degree in flow angle. Typically, the seed particles have lower velocities and lower flow angles.

REFERENCES

1. Moffitt, T. P., Stepka, F. S., and Rohlik, H. E., "Summary of NASA Aerodynamic and Heat Transfer Studies in Turbine Vanes and Blades," SAE Paper 760917, Nov. 1976.
2. Goldman, L. J., and Seasholtz, R. G., "Laser Anemometer Measurements in an Annular Cascade of Core Turbine Vanes and Comparison with Theory," NASA TP-2018, 1982.
3. Katsanis, T., "Fortran Program for Calculating Transonic Velocities on a Blade-to-Blade Stream Surface of a Turbomachine," NASA TN D-5427, 1969.
4. Katsanis, T., and McNally, W. D, "Revised Fortran Program for Calculating Velocities and Streamlines on the Hub-Shroud Midchannel Stream Surface of an Axial-, Radial-, or Mixed-Flow Turbomachine or Annular Duct, I - User's Manual," NASA TN D-8430, 1977.
5. Denton, J. D., and Singh, U. K., "Time Marching Methods for Turbomachinery Flow Calculation, Part I Basic Principles and 2D Applications and II Three-Dimensional Flows," VKI Lecture Series 1979-7, 1979.
6. Dodge, P. R., "3-D Heat Transfer Analysis Program," AFAPL-TR-77-64, Oct. 1977.
7. Seasholtz, R. G., and Goldman, L. J., "Laser Anemometer using a Fabry-Perot Interferometer for Measuring Mean Velocity and Turbulence Intensity along the Optical Axis in Turbomachinery," to be presented at the ASME Symposium of Engineering Application of Laser Velocimetry. Phoenix, Arizona, Nov.14-19, 1982.
8. Powell, J. A., Strazisar, A. J., and Seasholtz, R. G., "Efficient Laser Anemometer for Intra-Rotor Flow Mapping in Turbomachinery," Journal of Engineering for Power, Vol. 103, No.2, Apr. 1981, pp. 424-429.
9. Stevenson, W. H., dos Santos, R., and Mettler, S. C., "A Laser Velocimeter Utilizing Laser-Induced Fluorescence," Applied Physics Letters, Vol.27, no. 7, Oct. 1975, p. 395-396.
10. Goldman, L. J., Seasholtz, R. G., and McLallin, K. L., "Velocity Surveys in a Turbine Stator Annular-Cascade Facility using Laser Doppler Techniques," NASA TN D-8269, 1976.
11. Wolberg, J. R., Prediction Analysis, 1st ed., Van Nostrand, New Jersey, 1967.
12. Beck, J. V., and Arnold, K. J., Parameter Estimation in Engineering and Science, 1st ed., Wiley, New York, 1977.
13. Van Trees, H. L., Detection, Estimation, and Modulation Theory. Part I - Detection, Estimation, and Linear Modulation Theory, 1st ed., Wiley, New York, 1968.
14. Maxwell, B. R., "Particle Flow in Turbomachinery with Application to Laser Doppler Velocimetry," AIAA Journal, Vol.12, No.10, Oct. 1974, pp. 1297-1298.
15. Goldman, L. J., and McLallin, K. L., "Cold-Air Annular-Cascade Investigation of Aerodynamic Performance of Core-Engine-Cooled Turbine Vanes, I - Solid-Vane Performance and Facility Description," NASA TM X-3224, 1975.

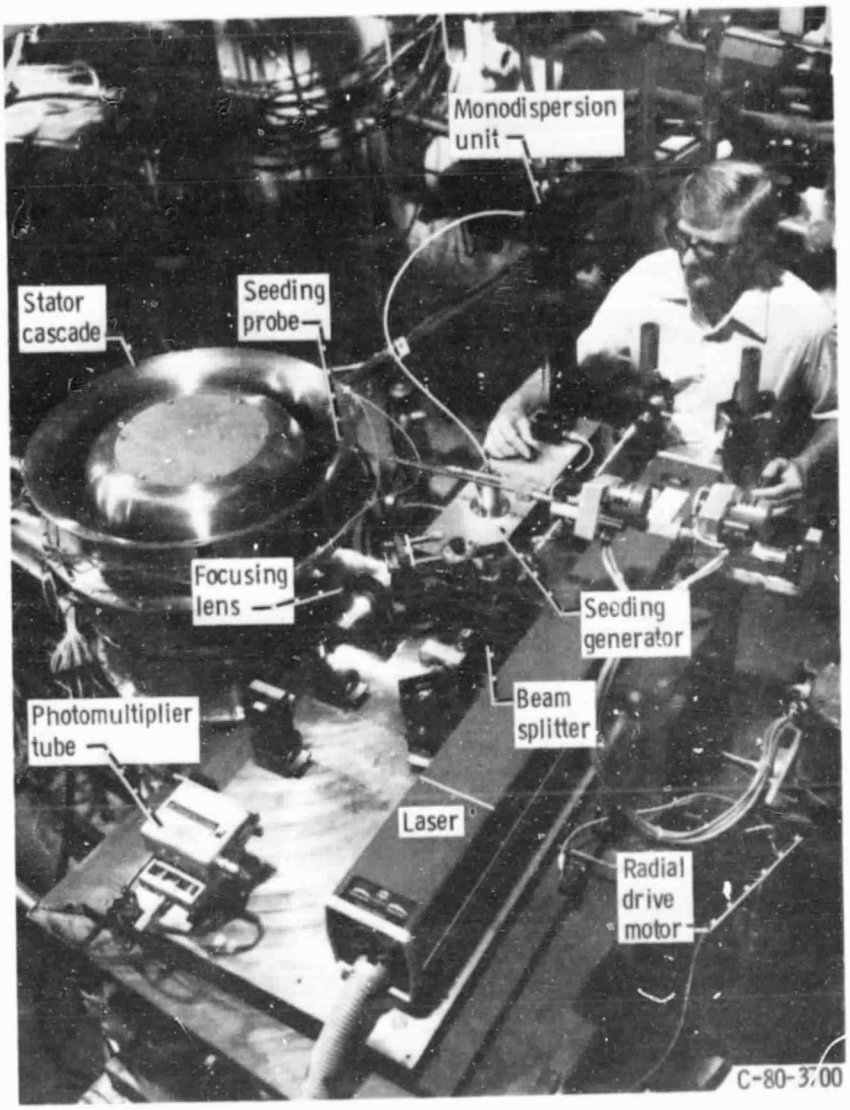

Figure 1. - Core stator annular cascade and laser anemometer.

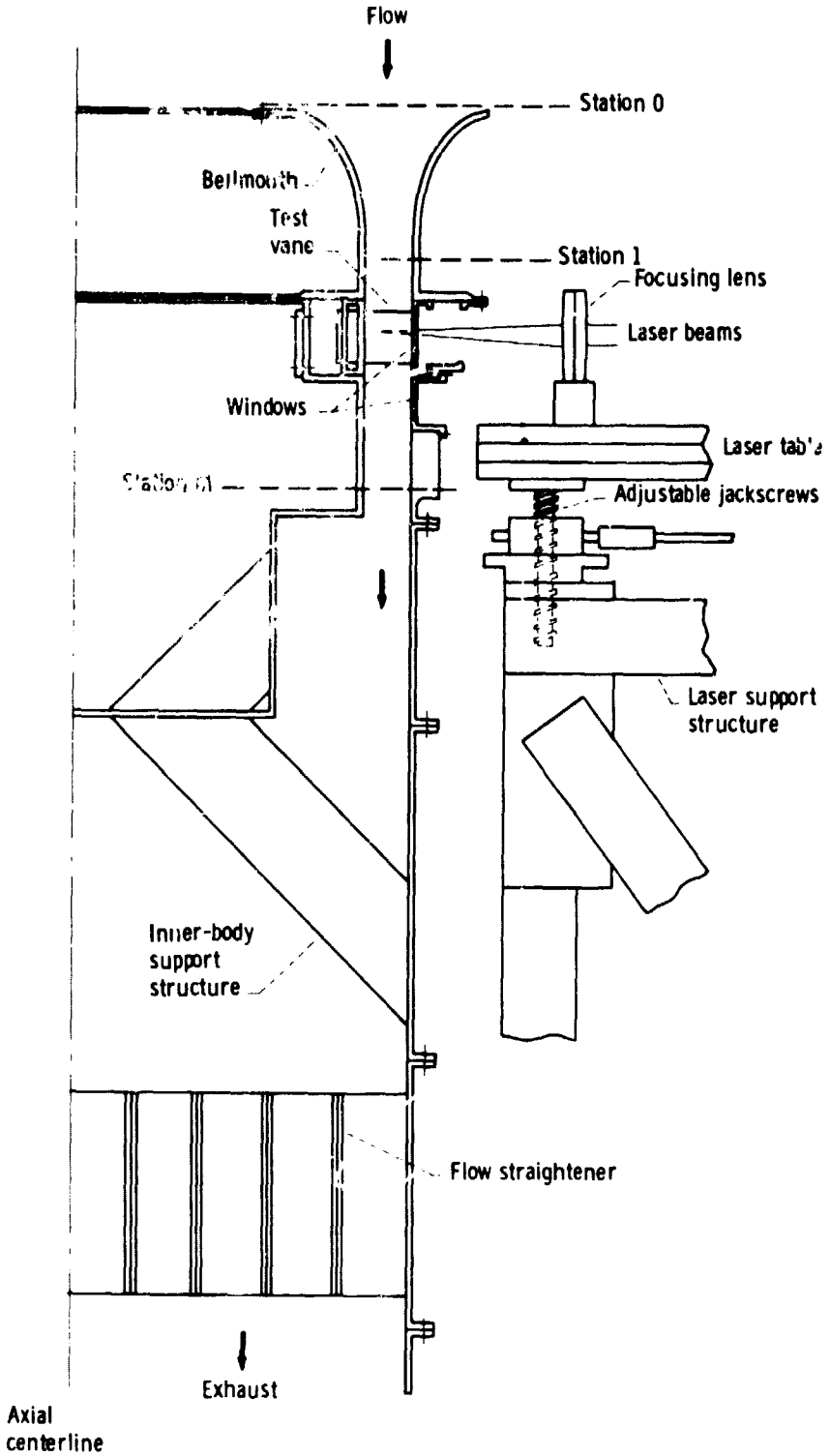

Figure 2. - Schematic cross-sectional view of core turbine stator cascade.

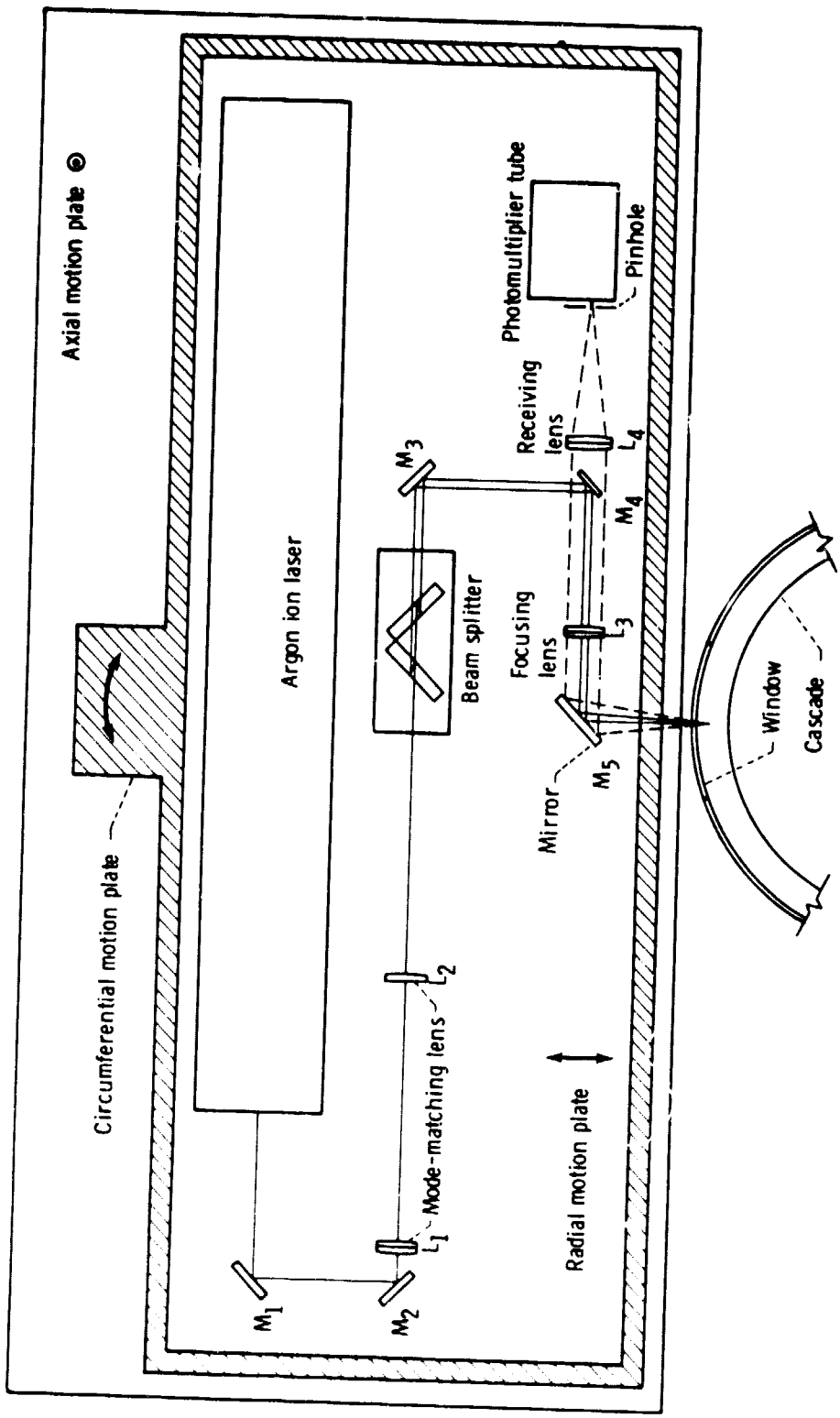

Figure 3. - Schematic of laser anemometer and transversing mechanism.

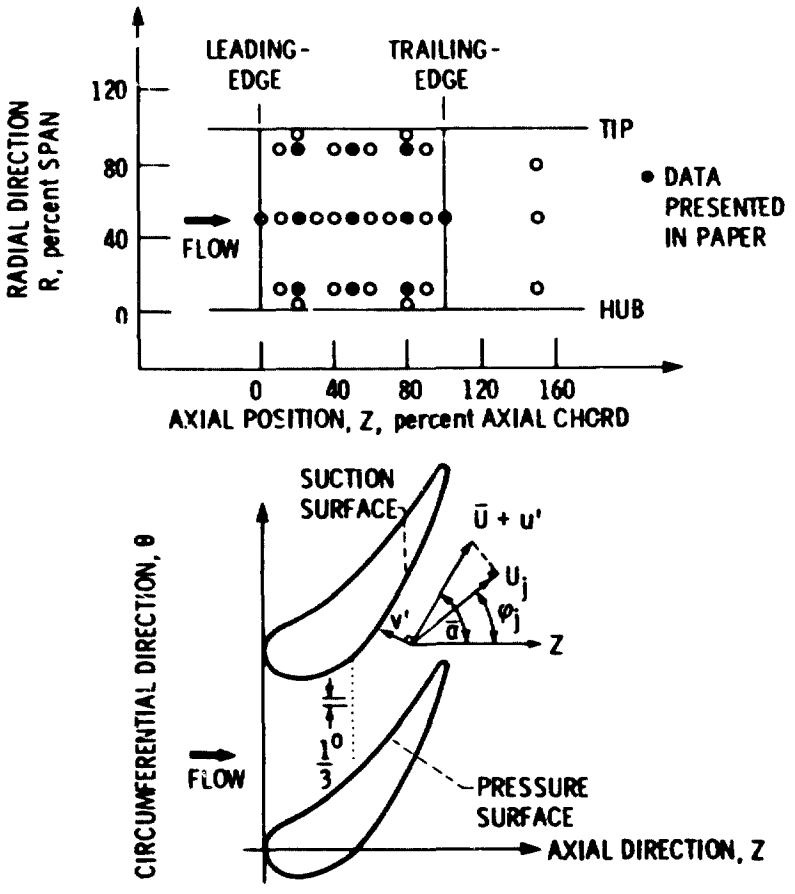

Figure 4. - Laser survey measurement locations and nomenclature.

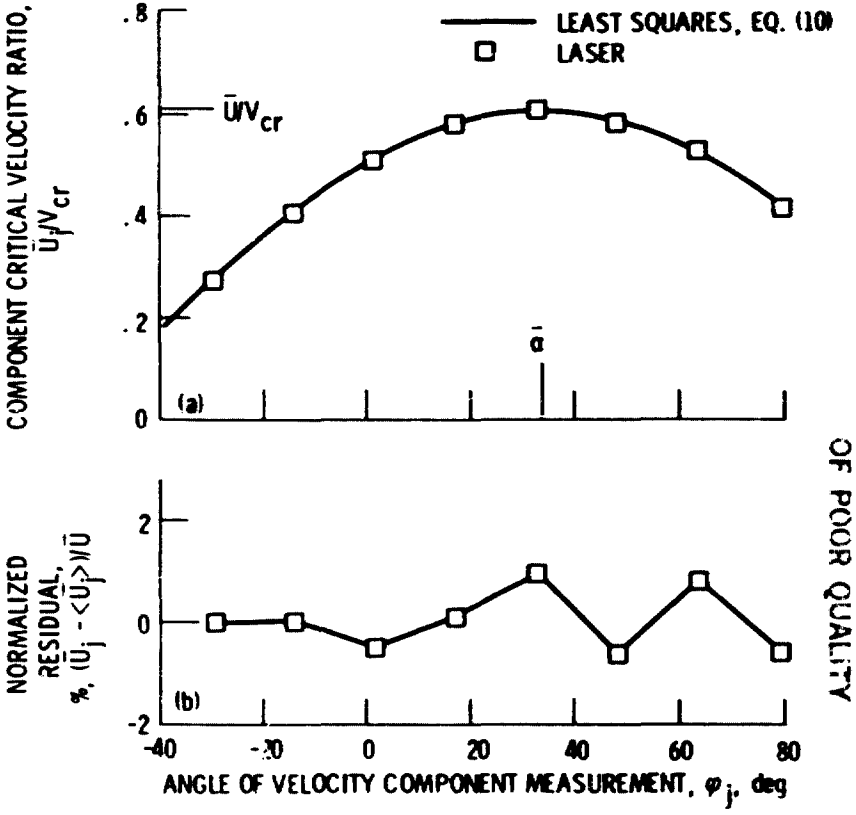

(a) Component critical velocity ratio.

(b) Residual.

Figure 5. - Parameter estimation of velocity magnitude and flow angle at 50% axial chord and 50% span.

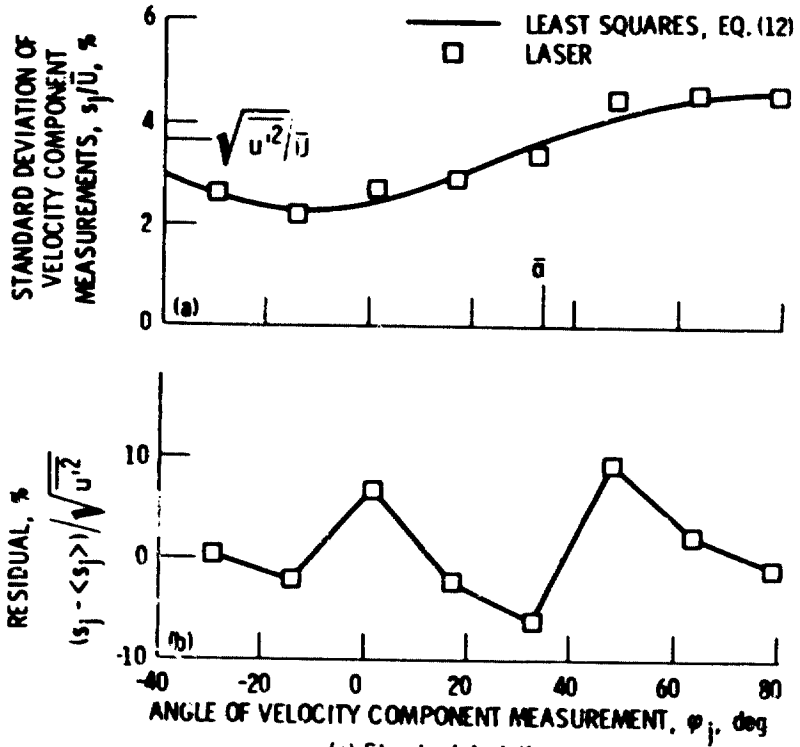

(a) Standard deviation.

(b) Residual.

Figure 6. - Parameter estimation of turbulent stresses at 50 % axial chord and 50 % span.

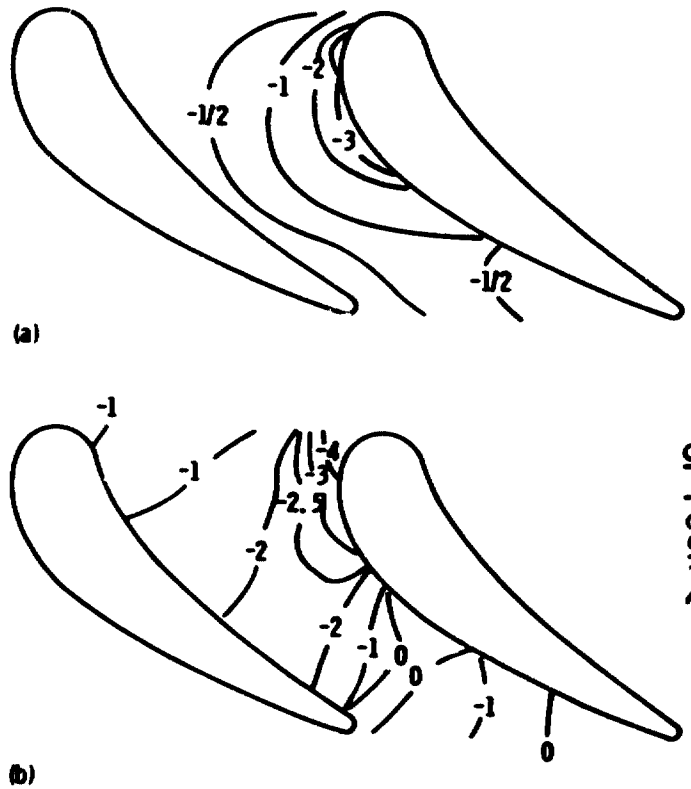

(a) Flow angle difference, $\alpha_P - \alpha_G$, deg.

(b) Velocity difference, $(V_P - V_G)/V_G$, percent.

Figure 7. - Dynamic behavior of 1.2 μm diam particles entrained in air flow through core turbine vanes at mean radius.

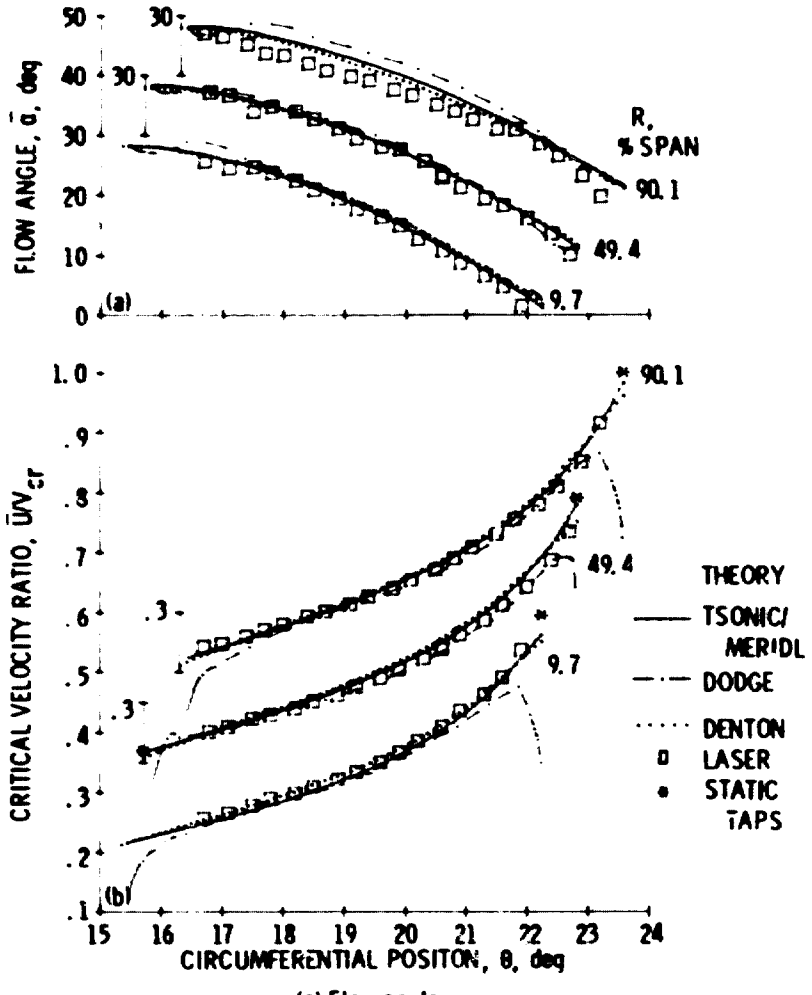

(a) Flow angle.

(b) Critical velocity ratio.

Figure 8. - Comparison of laser measurements with theory at 20.0 percent axial chord.

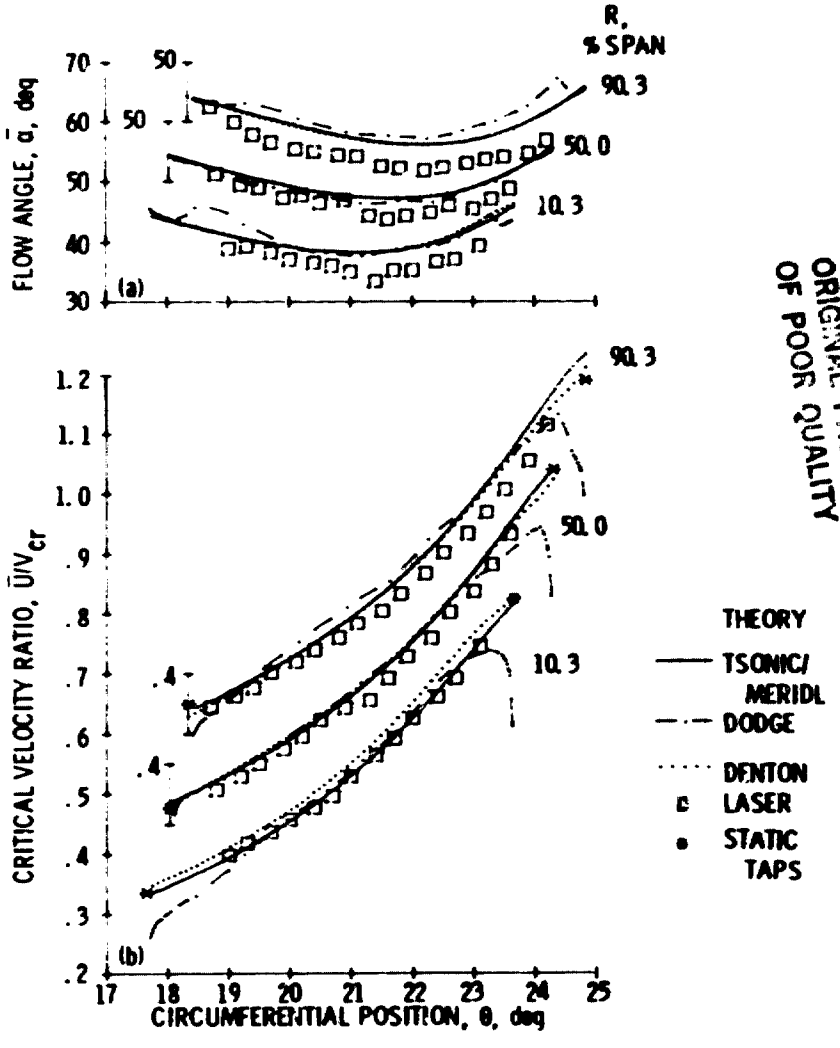

(a) Flow angle.

(b) Critical velocity ratio.

Figure 9. - Comparison of laser measurements with theory at 50.0 percent axial chord.

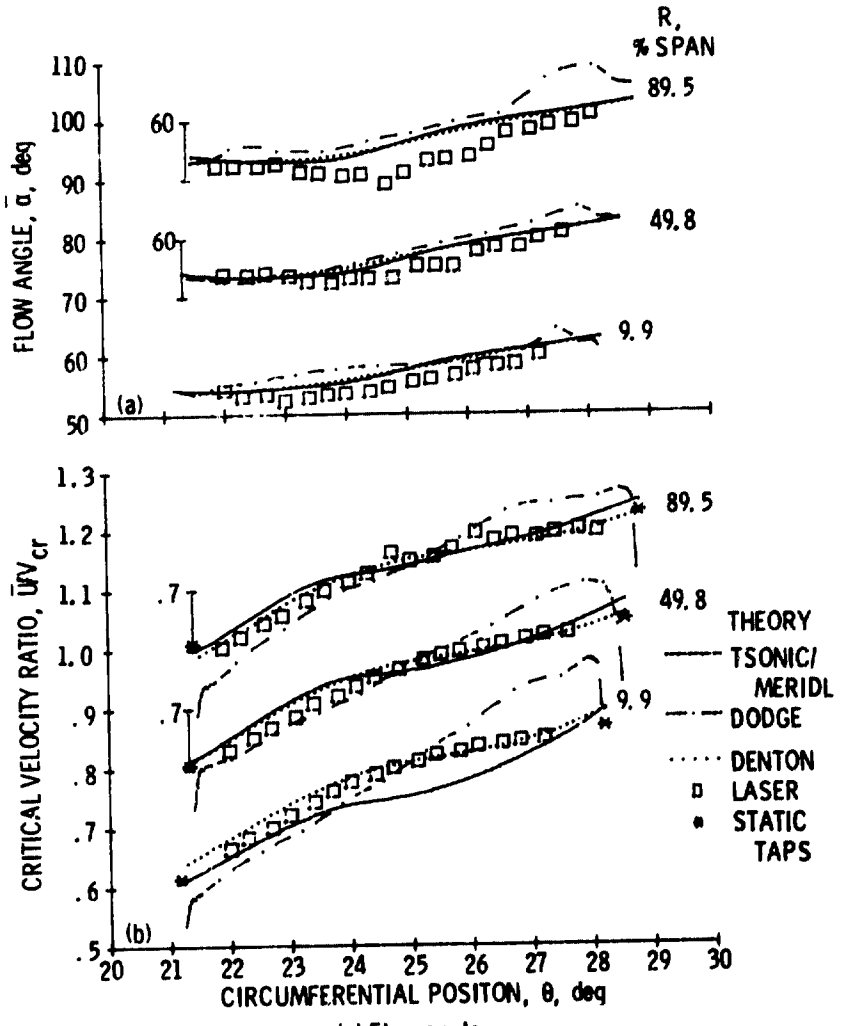

(a) Flow angle.

(b) Critical velocity ratio.

Figure 10. - Comparison of laser measurements with theory at 80.0 percent axial chord.